High-Speed TDoA Indoor Localization System With Aperture-Coupled Microstrip Patch Antennas

Silvio Marti[1], Hans-Dieter Lang[2], Heinz Mathis[2] and Hannes Diethelm[3]

[1]LEGIC Identsystems AG, Wetzikon, ZH, Switzerland
[2]OST – Eastern Switzerland University of Applied Sciences, Rapperswil, SG, Switzerland
[3]MOJO Devices, Stettbach, ZH, Switzerland

Abstract

Ultra-wideband (UWB) based localization systems became popular to navigate unmanned aerial vehicles (UAV) indoors, e.g. for light shows. The developed UWB localization system outperforms other systems due to the flexibility of the auto-calibration method for the anchor positions and the increased multipath resistance achieved with an aperture-coupled microstrip patch antenna. A dedicated Time Difference of Arrival (TDoA) based message exchange procedure allows a position update rate of up to 200 Hz with a constant measurement delay of 8.4 ms. Furthermore, the reliability is increased by including redundancy in the message exchange procedure. A standard deviation of the position within 3.5 cm is achieved with an operating range exceeding 100 m.

Keywords

Indoor Localization System, Ultra-Wideband, TDOA, Auto-calibration, Patch Antenna, Multipath

1. Introduction

Considerable research has been carried out to develop indoor localization systems for unmanned aerial vehicle (UAV) navigation in buildings, where no GNSS service is available. This includes vision-based systems, e.g. [1], which provide millimeter accuracy at the cost of expensive hardware and a high computational effort. Alternatively, centimeter-accurate approaches use pulse-based ultra-wideband (UWB) technology. In [2] and [3], two UWB-based indoor localization systems are presented. For light shows on stages, the rapidly changing light conditions prevent the usage of vision-based systems, which makes UWB the preferred technology.

Of the various challenges for UWB-based localization systems, the following three topics are addressed in this paper: Auto-calibration of the anchor positions and cable delays to apply the TDoA localization algorithm, the multipath problem with omnidirectional antennas, and the message exchange procedure to maximize the position update rate with constant measurement time and redundancy.

The remainder of this paper is structured as follows. Section 2 introduces the system architecture of the indoor navigation system. Section 3 deals with the anchor calibration. The auto-calibration algorithm proposed determines all cable delays and all anchor positions simultaneously based on only a small number of known coordinates. Section 4 deals with the UWB

IPIN 2021 WiP Proceedings, November 29 – December 2, 2021, Lloret de Mar, Spain
silvio.marti@legic.com (S. Marti); hansdieter.lang@ost.ch (H. Lang); heinz.mathis@ost.ch (H. Mathis)

antenna. This section lines out the limitations of the multipath detection with omnidirectional antennas and proposes a solution with an aperture-coupled microstrip patch antenna. In Section 5, a new TDoA message exchange procedure is presented, which allows a position update rate of 200 Hz and an independent measurement delay and contains redundancy to increase reliability. Finally, results are shown and conclusions are drawn in Section 6 and 7, respectively.

2. System Architecture

Fig. 1 shows the block diagram of the localization system. The central location engine (CLE)

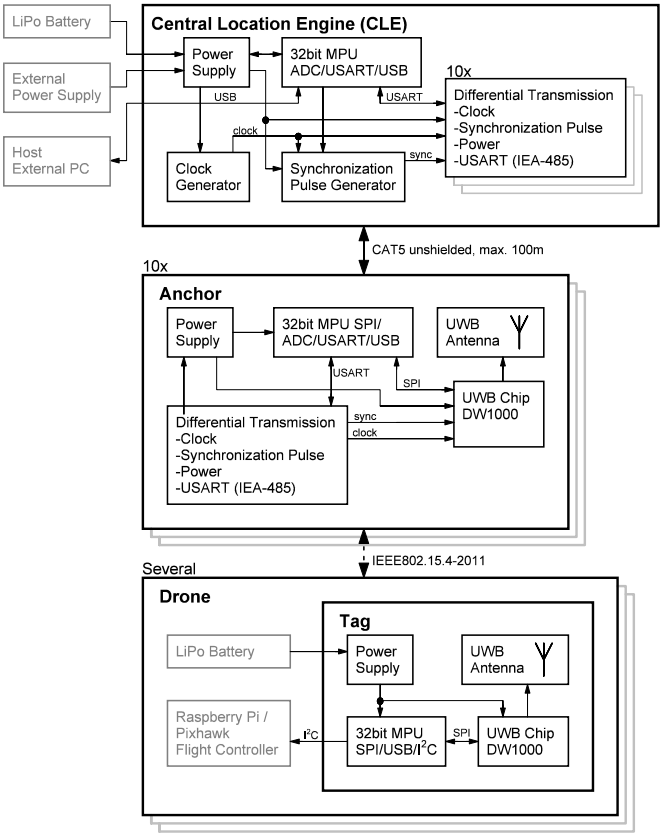

Figure 1: System architecture of the indoor localization system.

is the master device in the system. It controls all procedures and carries out all calculations. Furthermore, the CLE generates the reference clock using a temperature-compensated crystal oscillator (TCXO). The anchors in the proposed system are time-synchronized over cable to increase accuracy and position update rate, making air-time for clock synchronization unnecessary. The maximum cable length is limited to 100 m due to the attenuation of the clock signal.

The transceivers in the clock distribution network are chosen to minimize clock jitter; thus, no clock reprocessing is required. Each anchor consists of the DW1000 UWB chip, a microprocessor

and a UWB antenna. The tag is mounted on a UAV and consists the same elements. Fig. 2 shows the designed tag and anchor with the aperture-coupled microstrip patch antenna. Fig. 3 shows the UAV with the mounted tag.

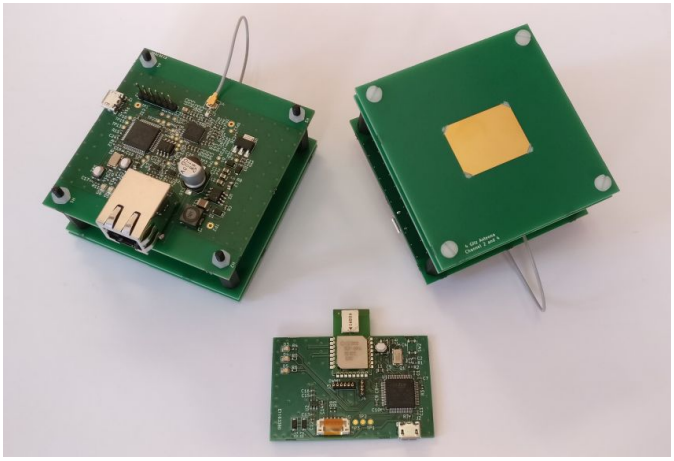

Figure 2: Front and rear view of the designed anchor with patch antenna and front view of the tag to be localized.

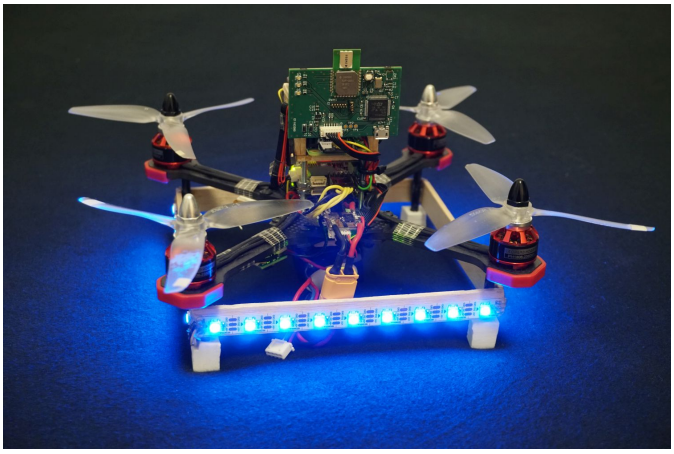

Figure 3: The UAV (drone) with the mounted tag PCB (green and the UWB chip antenna visible at the very top.

3. Anchor Calibration

To locate a tag, all anchor coordinates have to be known. Therefore, auto-calibration algorithms are used, because determining all coordinates manually on a stage is tedious work.

However, many auto-calibration algorithms either assume no prior knowledge about the anchor positions [3] or locate remaining anchors based and a few known anchors [4, 5]. Beyond

that, to use the system in TDoA mode, all cable delays τ_i have to be known as well. Typically, the cable delays have to be determined separately [6].

The auto-calibration algorithm proposed here solves several problems simultaneously. In many practical anchor constellations, certain anchor coordinates can often be easily measured, whereas others, possibly from the same anchor, cannot. The height above ground (z-coordinate) of an anchor hanging from the ceiling, for example, can be easily determined using a laser meter, unlike the x- and y-coordinates, which are more difficult to determine accurately. The best trade-off between the time required to set up the system and the accuracy of the auto-calibration algorithm is achieved when as many (easy to measure) coordinates as possible can be provided to the auto-calibration algorithm. Additionally, together with all unknown coordinates, all cable delays are determined at the same time.

Let A_1 to A_n denote all anchors, each with corresponding coordinates x_i, y_i, and z_i. The Euclidean distance $d_{i,j}$ between anchor i and j is calculated as

$$d_{i,j} = \sqrt{(x_j - x_i)^2 + (y_j - y_i)^2 + (z_j - z_i)^2}. \tag{1}$$

Fig. 4 illustrates an exemplary situation in which the auto-calibration algorithm is applied.

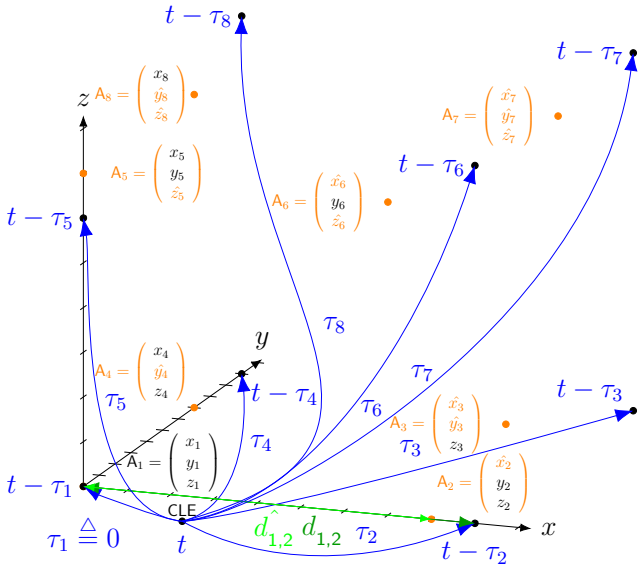

Figure 4: Example situation with eight anchors in a cube-like shaped setup. The black anchor nodes mark the true, (partially) unknown anchor positions. The orange nodes mark the estimated initial anchor positions. The time in each anchor A_i lags by τ_i with respect to the time at anchor A_1.

The eight true but partially unknown anchor positions are drawn as black nodes. The known coordinates (by definition or by measurement) can be selected individually for each anchor. For the remaining coordinates (denoted with a hat in the following), rough estimates have to be provided, for example by estimating the coordinates visually. The orange nodes mark the estimated initial values, which differ from the true, unknown black nodes. For this example, let anchor A_1 be the origin of the coordinate system by defining all coordinates of A_1 to be zero.

Suppose the anchors A_2, A_4, and A_5 lie on the x-, y-, and z-axis, respectively, and thus span a coordinate system together with A_1. This situation is represented by defining their yz-, xz-, and xy-coordinates, respectively, to be zero as well. Furthermore, assume it is known that the anchors A_3, A_6, and A_8 lie in the xy-, xz-, and yz-planes, respectively, which is achieved by fixing their z-, y-, and x-coordinates, respectively, to zero. Lastly, from anchor A_7, no coordinate is assumed to be known in this example.

It should be noted that if the anchors can be arranged in a constellation as shown in Fig. 4 and described in the aforementioned example, the system of equations will be well-conditioned without the need to measure a single distance. However, since, for example, the heights of anchors A_5 to A_8 can probably easily be measured using a laser meter, these coordinates could also be provided to the algorithm as known coordinates and would further increase the calibration accuracy.

The reference clock is generated on the CLE and distributed to all anchors via cables. However, since only the relative delays matter, τ_1 can be defined to be zero and hence all other delays, τ_2 to τ_n, refer to the time at anchor A_1. The estimated delays $\hat{\tau}_2$ to $\hat{\tau}_n$ can be initialized with zero.

In the following, it is described how the remaining coordinates and cable delays can be determined automatically. Let $t_{\text{tx},i}$ denote the time of transmission of a message from anchor A_i and let $t_{\text{rx},j,i}$ be the time of arrival of this message at anchor A_j. By measuring the timestamps for all k combinations of receivers and transmitters, the following system of equations can be formulated:

$$\left|\begin{array}{rcl} \hat{d}_{1,2}/c + \tau_1 - \hat{\tau}_2 & = & t_{\text{rx},2,1} - t_{\text{tx},1} \\ & \vdots & \\ \hat{d}_{1,n}/c + \tau_1 - \hat{\tau}_n & = & t_{\text{rx},n,1} - t_{\text{tx},1} \\ \hat{d}_{1,2}/c + \hat{\tau}_2 - \tau_1 & = & t_{\text{rx},1,2} - t_{\text{tx},2} \\ \hat{d}_{2,3}/c + \hat{\tau}_3 - \hat{\tau}_2 & = & t_{\text{rx},3,2} - t_{\text{tx},2} \\ & \vdots & \\ \underbrace{\hat{d}_{n-1,n}/c + \hat{\tau}_n - \hat{\tau}_{n-1}}_{f_k} & = & t_{\text{rx},n-1,n} - t_{\text{tx},n} \end{array}\right| . \tag{2}$$

Here, c refers to the speed of light and $\hat{d}_{i,j}$ to the Euclidean distance between anchor A_i and A_j based on the estimated coordinates. Thus, for the example illustrated in Fig. 4, $\hat{d}_{1,2}$ can be calculated as

$$\hat{d}_{1,2} = \sqrt{(\hat{x}_2 - x_1)^2 + (y_2 - y_1)^2 + (z_2 - z_1)^2}. \tag{3}$$

This nonlinear system of equations is solved using Newton's method. Therefore, partial derivatives have to be evaluated only for the estimated coordinates. The first equation of (2) for the example, illustrated in Fig. 4, then becomes

$$\underbrace{\frac{\hat{d}_{1,2}}{c} + \tau_1 - \hat{\tau}_2}_{f_1(\hat{x}_2,\hat{\tau}_2)} + \underbrace{\frac{\hat{x}_2 - x_1}{c\hat{d}_{1,2}}}_{\frac{\partial f_1(\hat{x}_2,\hat{\tau}_2)}{\partial \hat{x}_2}} \cdot \underbrace{\Delta x_2}_{x_2 - \hat{x}_2} + \underbrace{-1}_{\frac{\partial f_1(\hat{x}_2,\hat{\tau}_2)}{\partial \hat{\tau}_2}} \cdot \underbrace{\Delta \tau_2}_{\tau_2 - \hat{\tau}_2} \approx t_{\text{rx},2,1} - t_{\text{tx},1}. \tag{4}$$

Linearizing (2) in matrix form for the situation presented in Fig. 4, results in

$$\underbrace{\begin{bmatrix} \frac{\hat{x}_2-x_1}{c\hat{d}_{1,2}} & 0 & \dots & 0 & -1 & 0 & \dots & 0 \\ 0 & \frac{\hat{x}_3-x_1}{c\hat{d}_{1,3}} & \dots & 0 & 0 & -1 & \dots & 0 \\ \vdots & \vdots & \dots & \vdots & \vdots & \vdots & \dots & \vdots \\ \frac{\hat{x}_2-x_1}{c\hat{d}_{1,2}} & 0 & \dots & 0 & 1 & 0 & \dots & 0 \\ \frac{\hat{x}_2-\hat{x}_3}{c\hat{d}_{2,3}} & \frac{\hat{x}_3-\hat{x}_2}{c\hat{d}_{2,3}} & \dots & 0 & 1 & -1 & \dots & 0 \\ \vdots & \vdots & \dots & \vdots & \vdots & \vdots & \dots & \vdots \end{bmatrix}}_{\boldsymbol{A}} \cdot \underbrace{\begin{bmatrix} \Delta x_2 \\ \Delta x_3 \\ \vdots \\ \Delta z_5 \\ \Delta \tau_2 \\ \Delta \tau_3 \\ \vdots \\ \Delta \tau_8 \end{bmatrix}}_{\boldsymbol{x}} = \underbrace{\begin{bmatrix} t_{\text{rx},2,1} - t_{\text{tx},1} - \frac{\hat{d}_{1,2}}{c} - \tau_1 + \hat{\tau}_2 \\ t_{\text{rx},3,1} - t_{\text{tx},1} - \frac{\hat{d}_{1,3}}{c} - \tau_1 + \hat{\tau}_3 \\ \vdots \\ t_{\text{rx},1,2} - t_{\text{tx},2} - \frac{\hat{d}_{1,2}}{c} - \hat{\tau}_2 + \tau_1 \\ t_{\text{rx},3,2} - t_{\text{tx},2} - \frac{\hat{d}_{2,3}}{c} - \hat{\tau}_2 + \hat{\tau}_3 \\ \vdots \end{bmatrix}}_{\boldsymbol{b}}, \tag{5}$$

which is solved with the standard least squares method

$$\boldsymbol{x} = (\boldsymbol{A}^T\boldsymbol{A})^{-1}\boldsymbol{A}^T\boldsymbol{b}. \tag{6}$$

The estimated values are then updated according to

$$\begin{aligned} \hat{x}_2 &= \hat{x}_2 + \Delta x_2 \\ &\vdots \\ \hat{\tau}_8 &= \hat{\tau}_8 + \Delta \tau_8. \end{aligned} \tag{7}$$

Equations (5), (6) and (7) are evaluated until the Delta values fall below a predefined threshold, e.g., 1 mm.

4. UWB Antenna

UWB-based indoor localization systems typically use omnidirectional antennas [3, 2, 7], such as monopole chip antennas or cone antennas. Although the UWB technology is known to be insensitive to multipaths, not all multipaths can be detected with single omnidirectinal antennas. The system developed in [8] addresses this problem by utilizing an antenna array. This section highlights the limitations of the multipath detection with omnidirectional antennas and proposes a solution using a aperture-coupled microstrip patch antennas.

Multipaths can easily be detected in UWB systems if the length of the reflected path is at least one pulse length ct_p longer than the direct path d, where c equals the speed of light and t_p refers to the pulse length in time. For shorter multipaths, the direct and the reflected pulse overlap so that the multipath is no longer discernible. The radii a_M and b_M of the zone of undetectable multipaths can be calculated as

$$a_\text{M} = \frac{d + ct_\text{p}}{2}, \tag{8}$$

and

$$b_\text{M} = \sqrt{{a_\text{M}}^2 - \left(\frac{d}{2}\right)^2}. \tag{9}$$

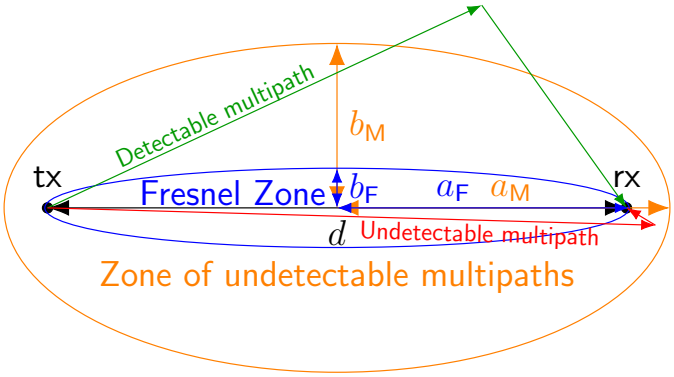

Figure 5: Zone of undetectable multipaths (for a pulse length of $t_p = 2\,\text{ns}$) and the Fresnel zone (for $f = 4\,\text{GHz}$) between two UWB transceivers separated by a distance of $d = 4\,\text{m}$.

Fig. 5 shows the zone of undetectable multipaths for two UWB transceivers. Additionally, an approximation of the first Fresnel zone is plotted, whose radii a_F and b_F can be calculated as

$$a_F = \frac{d}{2} + \frac{c}{4f} \tag{10}$$

and

$$b_F = \sqrt{\frac{dc}{4f}} \tag{11}$$

for the frequency of operation f.

It is remarkable that the zone of undetectable multipaths is significantly larger than the first Fresnel zone. Multipaths generated by reflections of objects outside the zone of undetectable multipaths (marked as *detectable multipath* in Fig. 5) show up as a separate pulse at the receiver and can thus be detected.

However, assume the transmitter of a UWB message is a UAV. Then, the direct path and the immediate vicinity of the UAV, apart from the UAV itself, is typically free of obstacles. Note that this is not necessarily true for the anchors, since they have to be attached to something, for example a tripod, a wall, or in the case of on-stage use, an aluminum truss. These objects, are likely to be in the zone of undetectable multipaths, behind the receiver. A multipath generated by such objects is illustrated with the red path (marked as *undetectable multipath*) in Fig. 5. Such a multipath can have a signal power comparable to the direct path, because the reflected path is only marginally longer. Furthermore, if the receiver antenna has an omnidirectional radiation pattern, signals from the direct path and a multipath can be received with similar antenna gain. Consequently, the reflected signal can significantly affect the signal from the direct path.

An elegant way to reduce the impact of reflections from the environment behind the anchor is to use an antenna whose radiation pattern has a zero at the back or at least only a small backlobe. In addition, the antenna should not have zeros in the front hemisphere. These requirements are fulfilled with the designed aperture coupled microstrip patch antennas, which have been successfully adopted for many wireless applications since their inception [9]. In this case, they are natural contenders for a multitude of reasons. First, it is well known that

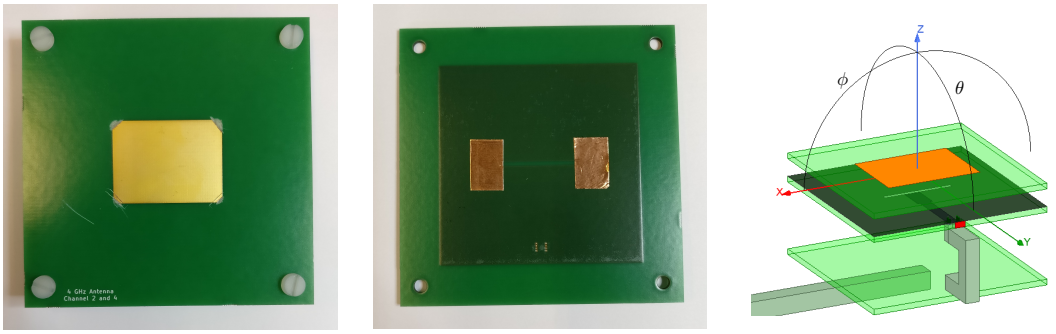

(a) (b) (c)

Figure 6: The designed 4 GHz anchor antenna: (a) tuned patch, (b) tuned slot and (c) simplified 3D model including cables.

they can provide a large enough bandwidth. Second, while their design methodology is rather straightforward, they also allow for easy tuning to comply with manufacturing tolerances and other uncertainties. Although still being electrically small overall, the ground planes should make the antenna characteristics less susceptible to influences of the cables. Two patch antennas have been designed, one for the 4 GHz IEEE 802.15.4 channels 2 and 4, and one for the 6.5 GHz channels 5 and 7. Fig. 6 shows the designed 4 GHz patch antenna and Tab. 1 lists the dimensions for both antennas.

Table 1
Parameters of the developed patch antennas (in mm).

Parameter	4 GHz Antenna	6.5 GHz Antenna
Patch length × width	20.0 × 26.3	12.7 × 19.7
Distance patch-aperture	4.9	2.1
Aperture (slot) length × width	19.3 × 1.1	15.2 × 0.9
Stub length × width	7.4 × 4.2	9.2 × 2.5

Fig. 8 shows the radiation pattern of the antennas. The front-to-back-ratio exceeds 20 dB, which makes the antenna significantly less sensitive to reflections from the back. The higher gain in the front direction compared to a monopole antenna has the additional advantage of increasing the operating range. Thus, a 90% two-way communication success ratio between anchors and tags has been achieved at a distance of 170 m.

5. Message Exchange Procedure

The goal of the message exchange procedure is to avoid collisions while maximizing the position update rate. Furthermore, redundancy shall be included to increase the reliability. The proposed UWB message exchange procedure is illustrated in Fig. 9 and can be described as follows: Let n denote the number of anchors and n_T denote the number of tags in the system, respectively. First, the CLE transmits previously calculated positions to the tags $\mathrm{T}_{(i-1) \bmod n}$, $\mathrm{T}_{(i-2) \bmod n}$ (if $n_\mathrm{T} \geq 3$), and $\mathrm{T}_{(i-3) \bmod n}$ (if $n_\mathrm{T} \geq 4$) via the anchor which has received the UWB message

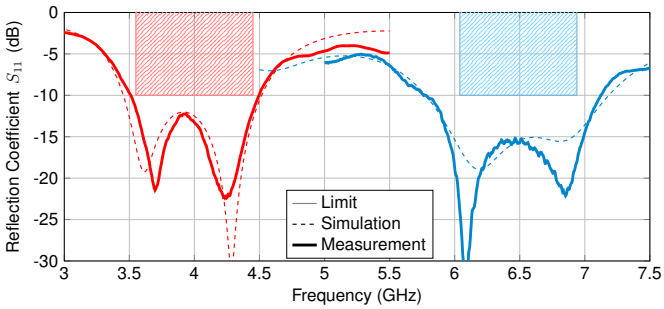

Figure 7: Comparison of the designed and measured impedance matching of the antenna for the IEEE 802.15.4 channels 2 and 4 (red) and of the antenna for the channels 5 and 7 (blue), respectively. The DW1000 receiving bandwidth for channel 4 is limited to 900 MHz. The reflection coefficient of the antenna is thus below -10 dB within the limited DW1000 bandwidth.

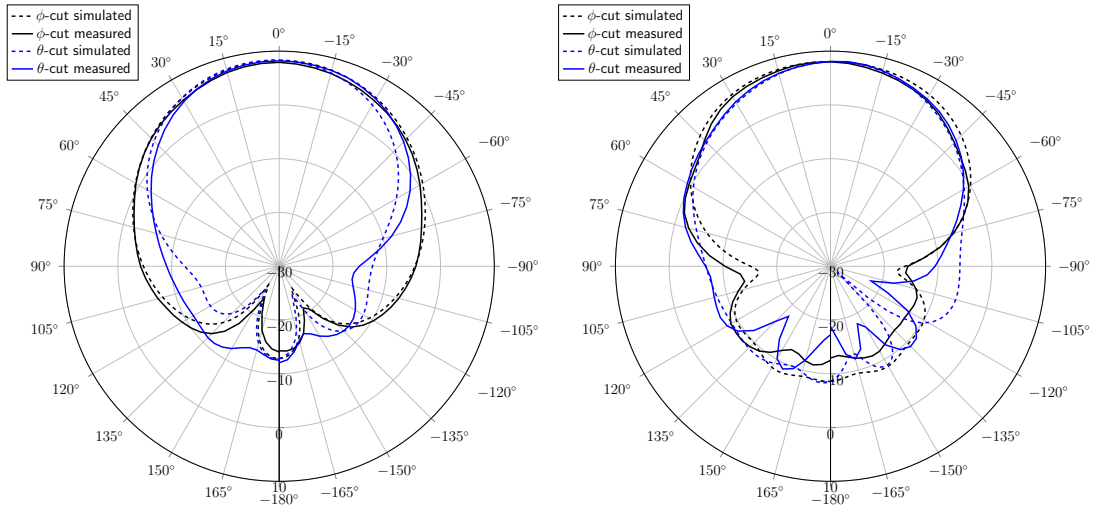

(a) (b)

Figure 8: Simulated and measured radiation pattern of the designed UWB patch antenna for the 4 GHz channels (2 and 4) in (a) and the 6.5 GHz channels (5 and 7) in (b) of the IEEE 802.15.4 standard, respectively. The radiation patterns are evaluated at the channel center frequencies, which are 3.9936 GHz and 6.4896 GHz, respectively. The coordinate system is shown in Fig. 6(c). Gain is expressed in dBi.

from tag $\mathrm{T}_{(i-1) \bmod n}$ with the highest signal strength. Then, tag $\mathrm{T}_{(i+1) \bmod n}$ transmits a UWB message (blink message), which is received and timestamped at all anchors. In the meantime, the CLE calculates the position of the tag T_i based on the timestamps recorded in the previous round. Next, the newly measured timestamps from tag $\mathrm{T}_{(i+1) \bmod n}$ are collected from all anchors. Finally, the counter variable i is updated according to

$$i = (i + 1) \mod n \tag{12}$$

and the procedure starts over. With a total time requirement of 5 ms per position, a position update rate of 200 Hz can be achieved.

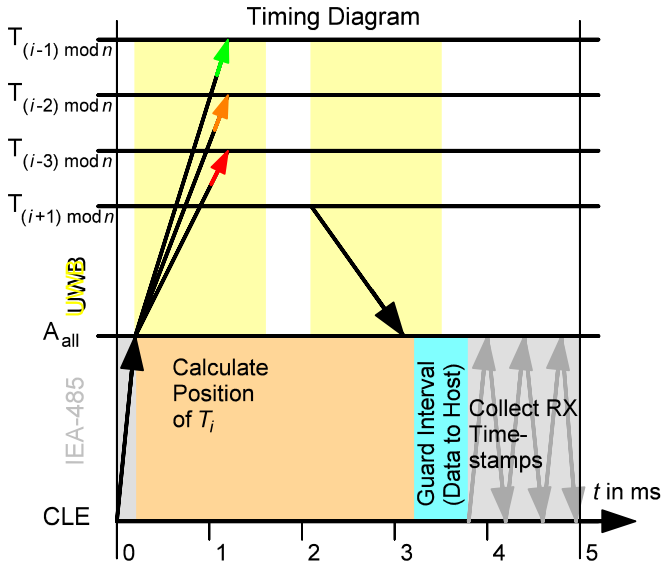

Figure 9: Periodic timing diagram of the message exchange procedure. In UWB messages, the arrow tip marks the time of reception of the time-stamped pulse, while the shaded area marks the total on-air time of the message.

This message exchange procedure contains redundancy to increase reliability. If a tag position is not received the first time (green arrow in Fig. 9), it will be retransmitted two additional times (orange and red arrows). The tag calculates the time until it retransmits its blink message depending on the attempt at which it has received its position and the total number of tags in the system.

The delay between the transmission of the timestamped pulse of a tag and the reception of the calculated position on the same tag is approximately 8.4 ms and it is independent of the total number of tags and anchors in the system. Such a low and constant latency is highly advantageous for the flight controller. In addition, the system is able to track fast-moving objects because the position can be calculated with only one UWB message.

6. Results

An absolute accuracy of 10 cm with respect to the ground truth can be achieved with a cube-shaped anchor constellation as shown in Fig. 10. Fig. 11 shows the histogram and the cumulative distribution function for localization measurements performed with an anchor constellation presented in Fig. 10. As can be observed, 68% and 95% of all positions lie within a sphere of radius $r = 3.5\,\text{cm}$ and $r = 6.3\,\text{cm}$, respectively. Up to 200 positions per second with a constant measurement delay of 8.4 ms can be determined with the proposed message exchange procedure. Due to the redundancy, the position can be determined in 99.5% of all cases. In the remaining cases, either not enough anchors have received the tag's blink message or the tag has not received the finally calculated position. The designed aperture-coupled microstrip

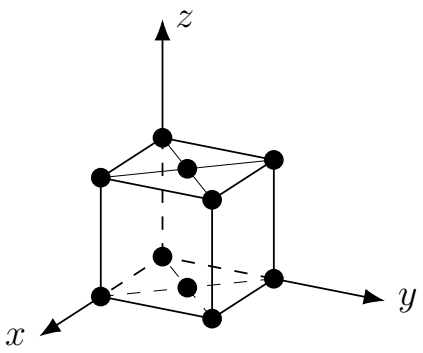

Figure 10: Anchor constellation for the results shown in Fig. 11. The side length of the cube is 1.8 m. The same true coordinates are provided as in the example described in Sec. 3, except that for the two additional anchors the z-coordinates are provided as well. The antennas are vertically polarized and directed to the center of the cube.

patch antenna increases immunity to multipaths generated by objects in close proximity to the transceivers and lets the operating range exceed 100 m.

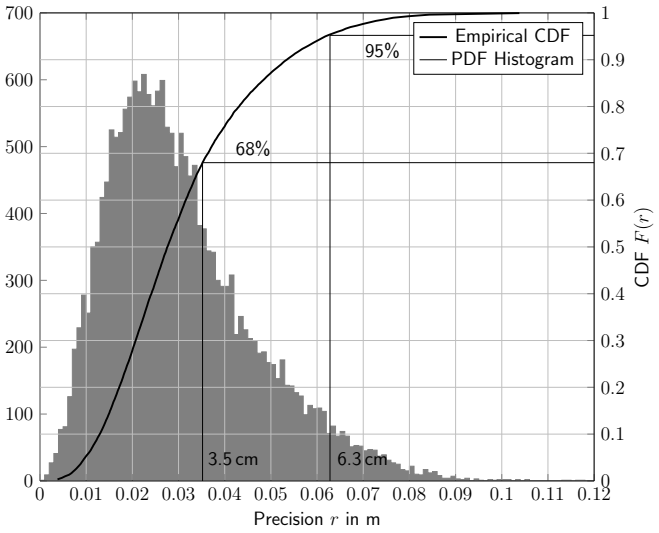

Figure 11: The precision of the proposed localization solution: Typical histogram and resulting cumulative distribution function (cdf) for a localization with an anchor constellation shown in Fig. 10.

7. Conclusions

Three typical issues for UWB-based indoor localization systems have been addressed in this paper. The auto-calibration algorithm proposed in Sec. 3 can determine unknown coordinates and cable delays at the same time. For each anchor position, it can be individually selected which coordinates are known or can be measured accurately. This makes the system suitable to

be used on a stage, where the anchor constellation can be complicated.

In Sec. 4, the limitations of the multipath detection in a UWB system with omnidirectional antennas are outlined. Immunity to reflections from objects in close proximity behind the anchors can be achieved by using aperture-coupled microstrip patch antennas because of their low backlobes. The higher gain in the region of interest additionally increases the operating range.

Finally, the message exchange procedure described in Sec. 5 contains redundancy and allows a position update rate of 200 Hz. In addition, every tag, independent of the total number of tags and anchors in the system, receives its position after a constant amount of time. All these properties make the proposed indoor localization system ideal for navigating fast-moving UAVs with a precision down to the size of an apple.

References

[1] S. Lupashin, M. Hehn, M. W. Mueller, A. P. Schoellig, M. Sherback, R. D'Andrea, A platform for aerial robotics research and demonstration: The flying machine arena, Mechatronics 24 (2014) 41–54.

[2] J. Tiemann, F. Schweikowski, C. Wietfeld, Design of an uwb indoor-positioning system for uav navigation in gnss-denied environments, in: 2015 International Conference on Indoor Positioning and Indoor Navigation (IPIN), 2015, pp. 1–7. doi:10.1109/IPIN.2015.7346960.

[3] K. Batstone, M. Oskarsson, K. Åström, Towards real-time time-of-arrival self-calibration using ultra-wideband anchors, in: 2017 International Conference on Indoor Positioning and Indoor Navigation (IPIN), 2017, pp. 1–8. doi:10.1109/IPIN.2017.8115885.

[4] Y. Yasukawa, Y. Higashi, A. Masuda, N. Miura, Automatic anchor caliburation for UWB-based indoor positioning systems, in: 2020 IEEE Region 10 Conference (TENCON), 2020, pp. 1374–1379. doi:10.1109/TENCON50793.2020.9293741.

[5] J. C. Chen, R. E. Hudson, K. Yao, Maximum-likelihood source localization and unknown sensor location estimation for wideband signals in the near-field, IEEE Transactions on Signal Processing 50 (2002) 1843–1854. doi:10.1109/TSP.2002.800420.

[6] P. Tomé, C. Robert, R. Merz, C. Botteron, A. Blatter, P.-A. Farine, UWB-based local positioning system: From a small-scale experimental platform to a large-scale deployable system, in: 2010 International Conference on Indoor Positioning and Indoor Navigation, 2010, pp. 1–10. doi:10.1109/IPIN.2010.5647454.

[7] B. Choi, K. La, S. Lee, UWB TDOA/TOA measurement system with wireless time synchronization and simultaneous tag and anchor positioning, in: 2018 IEEE International Conference on Computational Intelligence and Virtual Environments for Measurement Systems and Applications (CIVEMSA), 2018, pp. 1–6. doi:10.1109/CIVEMSA.2018.8439949.

[8] G. Schroeer, A real-time UWB multi-channel indoor positioning system for industrial scenarios, in: 2018 International Conference on Indoor Positioning and Indoor Navigation (IPIN), 2018, pp. 1–5. doi:10.1109/IPIN.2018.8533792.

[9] D. M. Pozar, Microstrip antenna aperture-coupled to a microstripline, Eletronics Letters 21 (1985) 49–50. doi:10.1049/el:19850034.